Supporting Information:

Nanoscale Carbon Modified α-MnO_2 Nanowires: Highly Active and Stable Oxygen Reduction Electrocatalysts with Low Carbon Content

*Julian A. Vigil,[†] Timothy N. Lambert, *[†] Jonathon Duay,[†] Collin J. Delker,[‡] Thomas E. Beechem,[§] and Brian S. Swartzentruber[‡]*

[†] Department of Materials, Devices & Energy Technologies,
[‡] Nanostructure Physics & Center for Integrated Nanotechnologies,
[§] Nanoscale Sciences Department,
Sandia National Laboratories; Albuquerque, New Mexico, USA, 87185.
** e-mail, tnlambe@sandia.gov; phone, 1 505 284 6967.*

Supporting Information (12 pp.)

Table of Contents

Figure S1	S-2
Figure S2	S-3
Figure S3 and Discussion	S-4 – S-5
Figure S4	S-6
Figure S5	S-7
Figure S6	S-8
Figure S7	S-9
Figure S8	S-10
Table S1	S-11
References	S-12

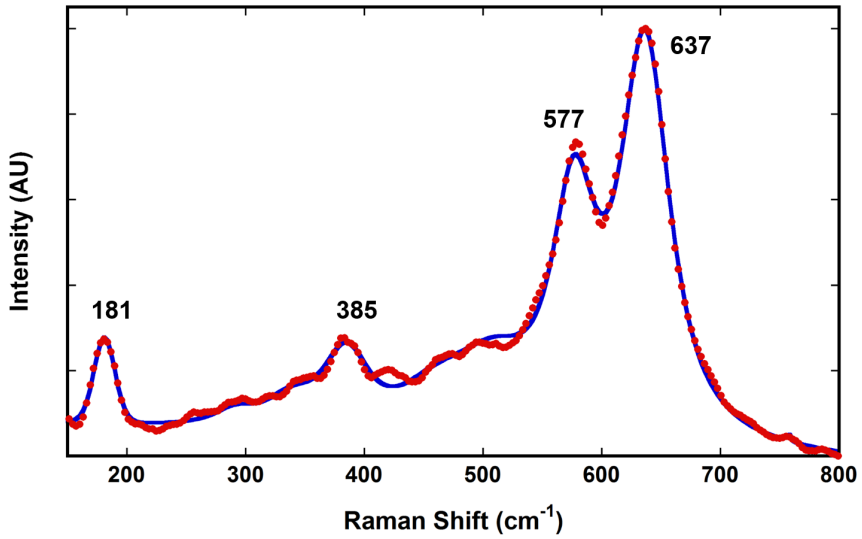

Figure S1. Raman spectrum of the C-MnO_2 NWs, where markers correspond to experimental data and the line is a composite fit incorporating all modes expected for α-MnO_2. Spectral positions of the major features are consistent with literature for α-MnO_2.[1]

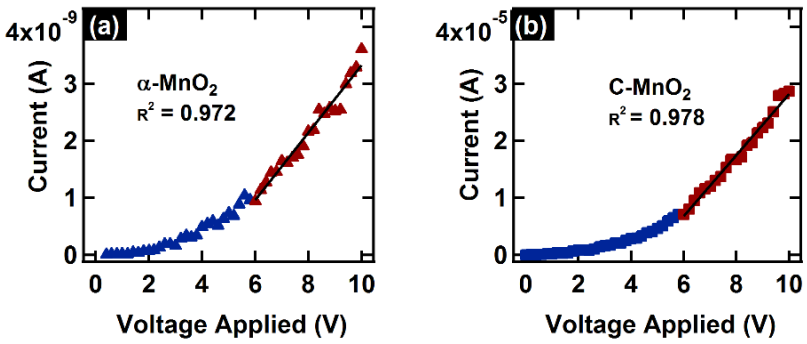

Figure S2. Representative *I-V* curves for the α-MnO_2 (a) and C-MnO_2 (b) nanowire devices. The data points shown in red were used to extract the resistance value from the given linear fit after activation of the device (blue points). See the Experimental Section for further details regarding the *I-V* characteristics.

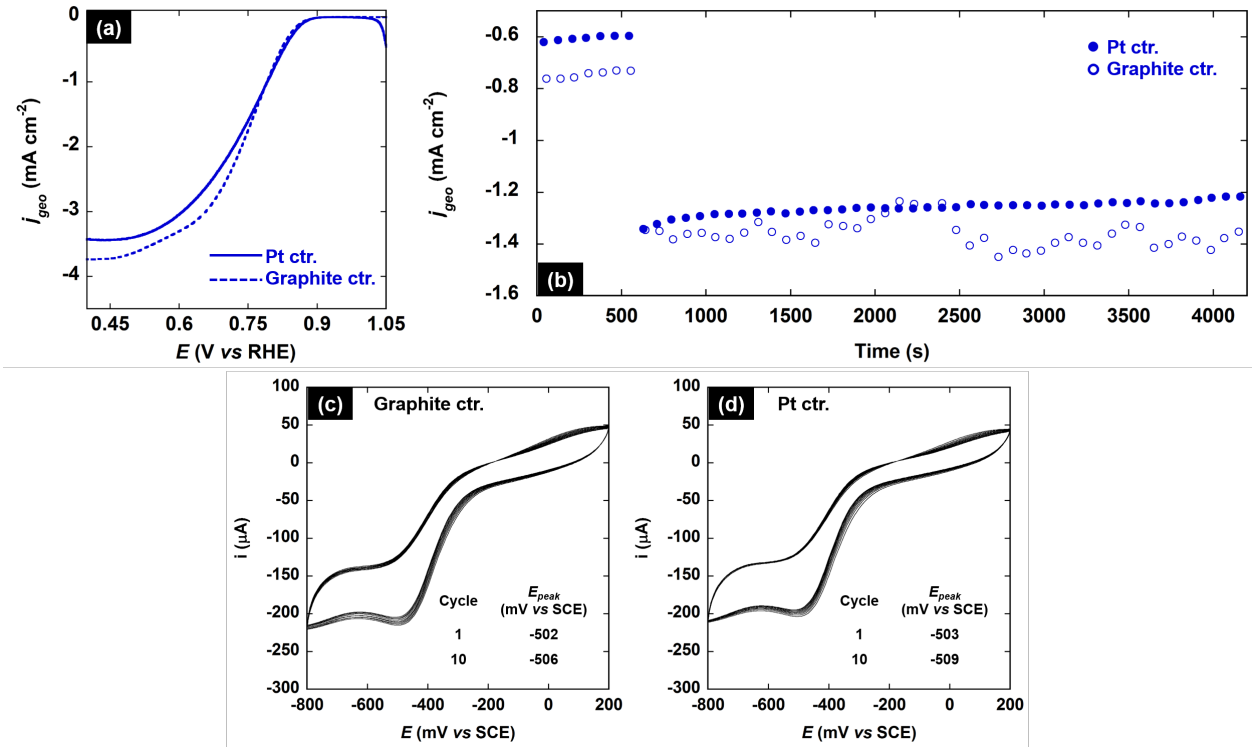

Figure S3. ORR RDE (a) and high-temperature chronoamperometry (b) experiments with the C-MnO_2 electrode were repeated under identical conditions to those reported in the main text (Figure 3a and 3e, respectively), with the exception that the standard Pt wire counter electrode was replaced with a graphite rod. Additionally, a C-MnO_2 electrode was cycled between 200 and -800 mV *vs* SCE (0.1 V s^{-1}, 100 RPM, O_2-sat. 0.1 M KOH) against a graphite rod (c) and Pt wire (d) counter electrode (inset: ORR peak potential for the first and last cycle).

Our group reported previously that no Pt was detected by X-ray fluorescence (XRF) measurements on a comparable Cu-α-MnO_2 working electrode after 24 h at a constant applied potential of ~ 0.65 V vs. RHE (O_2-sat. 0.1 M KOH, 2500 RPM) against an identical Pt wire counter electrode.[2] Here, the onset and half-wave potentials of the C-MnO_2 electrode against the graphite counter electrode are 0.87 and 0.75 V *vs.* RHE, respectively, within 10 mV of the corresponding C-MnO_2 electrode against a Pt counter electrode (Figure S3a, Table S1). The ORR peak potential is also within 5 mV between graphite and Pt counter electrodes for all cycles (Figures S3c, S3d). Finally, the activity and stability of the C-MnO_2 electrode is retained under high-temperature chronoamperometric conditions against a graphite counter electrode (Figure S3b). Thus, previous work and that presented in Figure S3 demonstrate there is no evidence (either electrochemically or spectroscopically) of Pt contamination at the working electrode, and the counter electrode composition has no appreciable effect on the ORR activity or stability of the C-MnO_2 NWs in scanning and cyclic RDE studies or high-temperature chronoamperometry. Small differences in activity are expected from "batch-to-batch" variation in synthesis and ink/electrode preparation.

This is not unexpected given that the limited literature on alkaline Pt dissolution show extremely slow rates: 2 – 8 x 10^{-11} g cm^{-2} h^{-1} in 1 M KOH at 1.05 V *vs* RHE.[3] Due to the rates being well below spectroscopic detection limits, reported values are often based on observed current and must assume quantitative conversion to the expected oxidized Pt species. Othman *et al.* reported no Pt detection (by AAS) in 0.1 or 1 M KOH electrolyte after 6 h of electrolysis on bulk Pt, which supports previous XRF results.[2,4] It is important to note that this literature concerns Pt working electrode dissolution. In contrast, the potential of the Pt wire counter electrode in the three-electrode ORR cell is not controlled or measured. The geometric surface area of the Pt wire counter electrode is also more than 50 times larger than the working electrode, thus reducing polarization at the interface with the electrolyte and dissolution characteristic of cycling across large potential windows.[5]

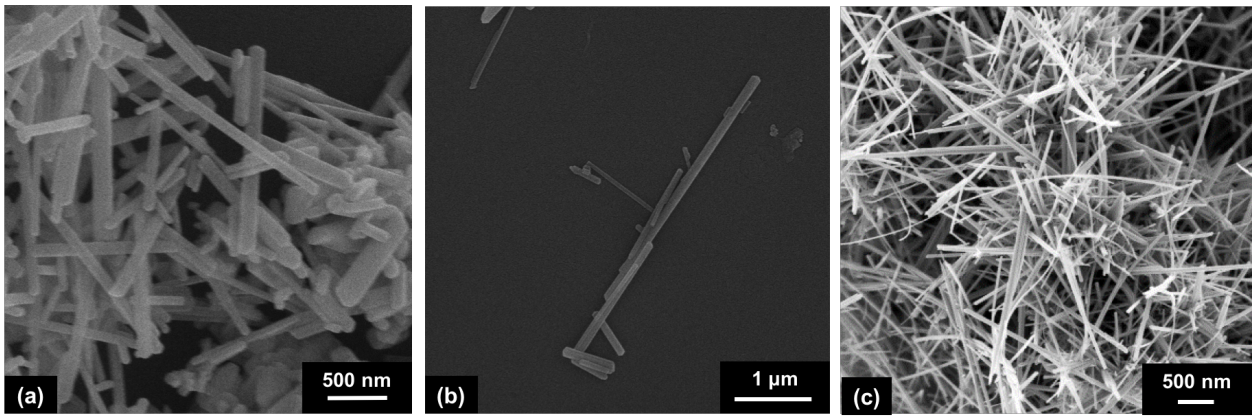

Figure S4. Additional SEM images of the bulk C-MnO_2 NWs, found in regions of aggregated wires (a) and isolated bundles (b), which demonstrate the observed wide distribution of nanowire lengths; (c) SEM image of the bulk α-MnO_2 NWs.

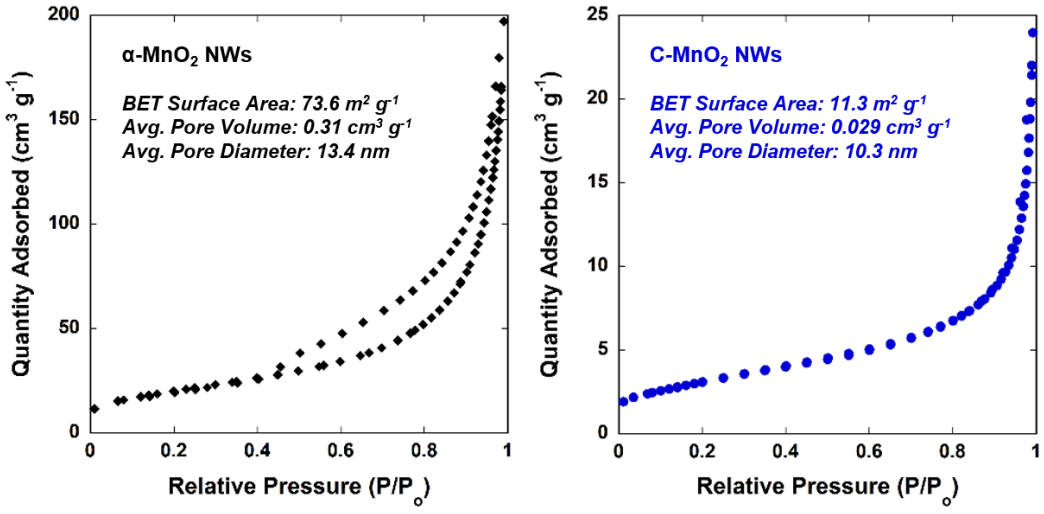

Figure S5. N_2 adsorption-desorption isotherms and calculated BET surface area, pore volume, and pore diameter for the α-MnO_2 (left) and C-MnO_2 (right) NWs.

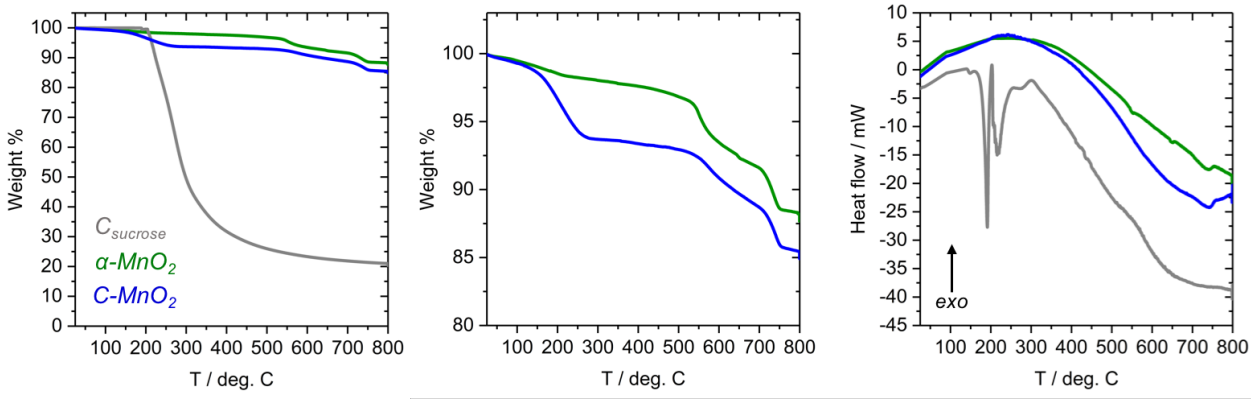

Figure S6. Thermogravimetric analysis (left, middle) and differential scanning calorimetry (right) analysis for a typical pyrolysis step (see Experimental Section of the main text). $C_{sucrose}$: pyrolysis of sucrose only (to form $C_{sucrose}$); α-MnO_2: pyrolysis of α-MnO_2 NWs only (to form Mn_xO_y); C-MnO_2: pyrolysis of 95 wt. % α-MnO_2 NWs: 5 wt. % sucrose (to form C-MnO_2).

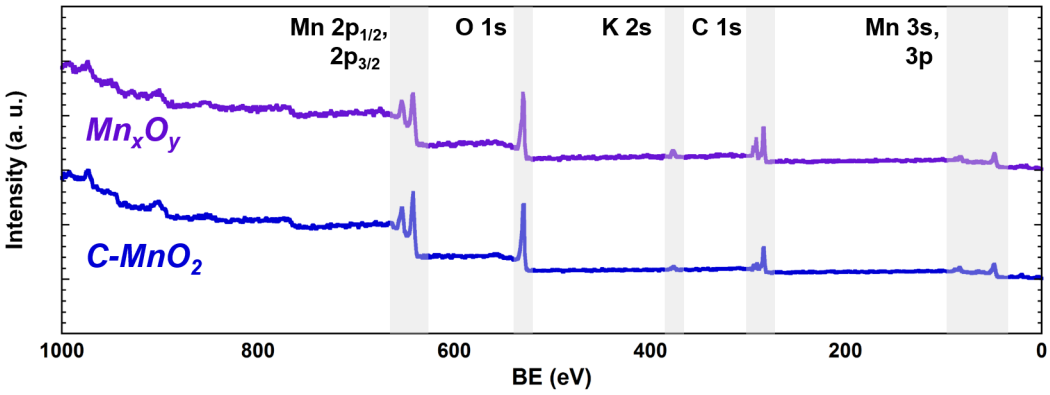

Figure S7. XPS survey spectra of the C-MnO_2 and Mn_xO_y NWs.

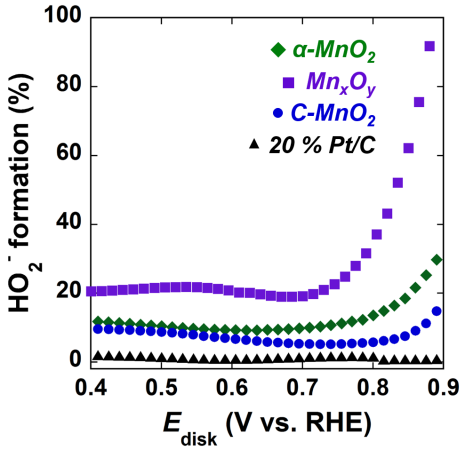

Figure S8. RRDE-derived peroxide generation ($\%_p$) in the ORR potential window for α-MnO_2, Mn_xO_y, C-MnO_2, and 20% Pt/C.

Table S1. Electrocatalytic ORR activity comparison of state-of-the-art carbon-coated electrocatalysts in alkaline media.

Catalyst	Ref.	Mass loading (mg cm^{-2})	C comp. (wt. %)	Conditions	Onset potential (V *vs* RHE)	Half-wave potential (V *vs* RHE)	Diffusion-limited geometric current density (mA cm^{-2})	*n* (e-)
Carbon-coated oxides								
C-MnO_2 NWs	this work	0.177	≤ 1.2	0.1 M KOH/ 2500 RPM	0.88 **	0.75	3.4	3.84
$BaMnO_3$@5%C	6	NR	NR	0.1 M KOH/ 1600 RPM	0.71	0.61	5.5	3.8
Mn_3O_4@CN_x	7	0.59 – 0.66	28.5	0.1 M KOH/ 1600 RPM	0.86	0.79	1.1	4 *
ND-Fe_3O_4@mC-2 /CB	8	0.1	65 ***	0.1 M KOH/ 1600 RPM	0.77	0.69	5.25	3.72
Carbon-coated metals, sulfides, phosphides								
PdCo@NPNCs	9	0.202	NR	0.1 M KOH/ 1600 RPM	0.95	0.91	5	>3.75
PC-$CoS_{1.097}$	10	0.566	24.8	0.1 M KOH/ 2400 RPM	0.89	0.84	3.7	>3.8
FeP@NPCs	11	0.2	88 ****	0.1 M KOH/ 1600 RPM	0.91	0.82	5.85	>3.75

NR = not reported; * reported *n* values calculated using the Koutecky-Levich method exceed the theoretical limit of 4 at some potentials; ** onset potential calculated using the tangential method, which may underestimate the value compared to the literature[2]; *** total C comp. = 60 wt % carbon black + 14.5 wt % of the remaining 40 wt % ND-Fe_3O_4@mC-2 catalyst = 65.8 wt % C; **** 88 at %.

References.

1. Gao, T.; Fjellvåg, H.; Norby, P. A comparison study on Raman scattering properties of α- and β-MnO2. *Anal. Chim. Acta* **2009,** *648* (2), 235-239.
2. Davis, D. J.; Lambert, T. N.; Vigil, J. A.; Rodriguez, M. A.; Brumbach, M. T.; Coker, E. N.; Limmer, S. J. Role of Cu-Ion Doping in Cu-α-MnO2 Nanowire Electrocatalysts for the Oxygen Reduction Reaction. *J. Phys. Chem. C* **2014**, *118*, 17342-17350.
3. Kolotyrkin, Y. M.; Losev, V. V.; Chemodanov, A. N. Relationship between corrosion processes and oxygen evolution on anodes made from noble metals and related metal oxide anodes. *Materials Chemistry and Physics* **1988**, *19*, 1-95.
4. Othman, M. R.; Riyanto Electrochemical Stability of Cu, Ni, Co, Pt and Ir Metals Sheet and Their Composite Electrodes in Potassium Hydroxide Solution. *Int. J. Electrochem. Sci.* **2012**, *7*, 8408-8419.
5. Cherevko, S.; Zeradjanin, A. R.; Keeley, G. P.; Mayrhofer, K. J. J. A Comparative Study on Gold and Platinum Dissolution in Acidic and Alkaline Media. *J. Electrochem. Soc.* **2014**, *161*, H822-H830.
6. Xu, Y.; Tsou, A.; Fu, Y.; Wang, J.; Tian, J.-H.; Yang, R. Carbon-Coated Perovskite $BaMnO_3$ Porous Nanorods with Enhanced Electrocatalytic Perporites for Oxygen Reduction and Oxygen Evolution. *Electrochim. Acta* **2015**, *174*, 551-556.
7. Gao, S.; Geng, K. Facile construction of Mn_3O_4 nanorods coated by a layer of nitrogen-doped carbon with high activity for oxygen reduction reaction. *Nano Energy* **2014**, *6*, 44-50.
8. Lida, H.; Elaheh, D.; Douglas, G. I.; Jonathan, G. C. V. Microwave-assisted synthesis and prototype oxygen reduction electrocatalyst application of N-doped carbon-coated Fe_3O_4 nanorods. *Nanotechnology* **2017**, *28*, 095707.
9. Zhang, Z.; Liu, S.; Tian, X.; Wang, J.; Xu, P.; Xiao, F.; Wang, S. Facile synthesis of N-doped porous carbon encapsulated bimetallic PdCo as a highly active and durable electrocatalyst for oxygen reduction and ethanol oxidation. *J. Mater. Chem. A* **2017**, *5*, 10876-10884.
10. Bai, F.; Huang, H.; Hou, C.; Zhang, P. Porous carbon-coated cobalt sulfide nanocomposites derived from metal organic frameworks (MOFs) as an advanced oxygen reduction electrocatalyst. *New J. Chem.* **2016**, *40*, 1679-1684.
11. Zhang, R.; Zhang, C.; Chen, W. FeP embedded in N, P dual-doped porous carbon nanosheets: an efficient and durable bifunctional catalyst for oxygen reduction and evolution reactions. *J. Mater. Chem. A* **2016**, *4*, 18723-18729.